Nanomed J. 12(1): 99-109, Winter 2025

RESEARCH PAPER

Formulation, optimization, and characterization of naringenin-loaded halloysite nanotube to achieve enhanced antioxidant and anticancer properties

Hamed Hamedinasab [1], Hossein Sabahi [1], Morteza Hosseini [1]*, Ali Hossein Rezayan [1]*

[1]Division of Nanobiotechnology, Department of Life Science Engineering, Faculty of New Sciences and Technologies, University of Tehran, Tehran, Iran

ABSTRACT

Objective(s): Poor solubility and stability of naringenin result in its low bioavailability. Halloysite nanotubes (HNTs) were investigated as a potential carrier for the controlled delivery of naringenin to HT-29 (human colon adenocarcinoma) and MCF-7 (human breast cancer) cell lines.

Materials and Methods: Naringenin was loaded in HNTs at different HNTs: drug ratios (w/w) of 30, 24, 16, 8, and 4, then characterized by SEM (Scanning electron microscope), FTIR (Fourier transform infrared spectroscopy), DSC (Differential scanning calorimetry), and XRD (X-ray diffraction). The effect of naringenin loaded in HNTs on its solubility was investigated by an innovative change in the DPPH (2, 2-diphenyl-1-picrylhydrazyl) assay. Cytotoxicity of naringenin and naringenin-loaded HNTs was investigated by MTT assay.

Results: At a ratio of 30, the highest encapsulation efficiency (87.7± 5%), and at a ratio of 4, the highest loading capacity was obtained (12± 0.6%). The drug release study indicated prolonged drug release from naringenin-loaded HNTs (67±5% after 24h). Naringenin showed antioxidant activity by scavenging DPPH radical with an IC50 value of 400 ±4 µg/mL. Naringenin solubility after loading was considerably increased and subsequently, showed 2.2-fold higher antioxidant activity than the free drug. Cytotoxicity assay indicated the anticancer activity of naringenin was significantly improved after loading.

Conclusion: HNTs can be a promising carrier for the delivery of naringenin.

Keywords: *Antioxidants, Clay, Drug delivery systems, Nanoparticles*

How to cite this article

Hamedinasab H, Sabahi H, Hosseini M, Hossein Rezayan A. Formulation, optimization, and characterization of naringenin-loaded halloysite nanotube to achieve enhanced antioxidant and anticancer properties. Nanomed J. 2025; 12(1): 99-109. DOI: 10.22038/nmj.2024.78609.1921

INTRODUCTION

Naringenin (5, 7-dihydroxy-2-(4-hydroxyphenyl) chroman-4-one) is a natural flavonoid that is widely distributed in a variety of fruits (blood orange, grapes, lemons, grapefruit, pummelo, and tangerines), vegetables and herbs [1, 2]. Its pharmaceutical effects include antioxidant, anticancer, anti-inflammatory, hepatoprotective, antifibrogenic, and antiatherogenic [3-6]. Hydroxyl groups of naringenin are responsible for its antioxidant property. Aromatic rings in naringenin have three hydroxyl groups which react with reactive oxygen species (ROS) by donating hydrogen [7]. Naringenin has anticancer effects on cell lines such as the breast, liver, colon, and uterus by inducing apoptosis in the cancer cells, but shows no cytotoxic effects on normal cells [3-6]. Poor water solubility, instability, and propensity to gastrointestinal degradation results in low permeability, low bioavailability (5.81% for oral administration), and extensive first-pass metabolism. These in turn restrict the clinical applications and in vivo biological effects of naringenin [8, 9]. By using a drug delivery system, much effort has been made to overcome the clinical restrictions of naringenin and improve its efficiency [10]. Drug delivery systems such as solid lipid nanoparticles (SLN) [10], polymer-nanoparticles [11, 12], and inorganic nanoparticles [12] have been studied. Nanoparticles have been widely used recently for increasing solubility,

* *Corresponding authors: Emails: hsabahi@ut.ac.ir; hosseini_m@ut.ac.ir*

Note. This manuscript was submitted on March 8, 2024; approved on May 21, 2024

bioavailability, and the efficacy of drugs [13-16]. By loading naringenin in sulfobutylether-cyclodextrin/chitosan nanoparticle, not only the solubility of naringenin was increased but also the residence time for local ocular mucosa was prolonged [17]. Naringenin was encapsulated in SLN aiming to increase the solubility and bioavailability of naringenin for pulmonary delivery. Encapsulation of naringenin in SLN increased its bioavailability 2.53-fold greater in comparison with naringenin suspension after pulmonary administration [10]. One of the nanocarriers used for drug delivery is Halloysite nanotubes (HNTs). HNTs as a natural clay with Al2Si2O5 (OH)4.2H2O formula and tubular structure. The inner lumen diameter, outer diameter, and length of HNTs are 12-15 nm, 50-70, and 500-1000 nm, respectively. The presence of silica and alumina on the outside and inside surfaces is responsible for the negative and positive charge of the outside surface and the inner lumen, respectively [18-27]. Due to safe and biocompatible properties of HNTs, they are used as a natural nanocarrier for the sustained release of drugs. HNTs have been utilized for the loading of tetracycline, khellin, nicotinamide adenine dinucleotide, 5-aminosalicylic acid, Brilliant green, ibuprofen, diphenhydramine hydrochloride, diclofenac sodium salt, ofloxacin, aspirin, and curcumin [18, 20-28]. But HNTs have not yet been used for delivery of naringenin. The hydrophilic nature, stability in physiological medium, low cost, natural nature, low toxicity, and sustained release of drug are advantages of HNTs that encouraged us to use it for delivery of naringenin.

In this study, naringenin was loaded in HNTs nanotube at HNTs:drug ratios (w/w) of 30, 24, 16, 8 and 4 to find the best condition for drug loading, and then characterized by SEM (Scanning electron microscope), FTIR (Fourier transform infrared spectroscopy), DSC (Differential scanning calorimetry), and XRD (X-ray diffraction). The effect of naringenin loaded in HNTs on its solubility was investigated by an innovative change in the DPPH (2, 2-diphenyl-1-picrylhydrazyl) assay. The anticancer activity of naringenin and naringenin-loaded HNTs on HT-29 (human colon adenocarcinoma) and MCF-7 (human breast cancer) cell lines was evaluated by MTT assay.

METHODS AND MATERIALS

Materials

Naringenin (purity; 95%) and HNTs were purchased from Sigma Aldrich. Absolute Ethanol (purity, 99.9%), DMSO (purity; 99.9%), Methanol (purity; ≥ 99.9%) and Glacial acetic acid (purity; 99.8-100.5%) were purchased from Merck. Sodium chloride (purity; ≥ 99%), Potassium chloride (purity; 99.5-100.5%), Sodium phosphate dibasic (purity, ≥ 99%), Potassium phosphate monobasic (purity; ≥ 99%), Dulbecco's Modified Eagle Medium (DMEM) and DPPH were purchased from Sigma Aldrich. HT-29 and MCF-7 cell lines were purchased from Pasteur Institute of Iran.

Methods

Loading process

Naringenin was loaded into various amounts of HNTs via the method described in a previous study [29]. 50 mg of naringenin was dissolved in 50 mL of absolute ethanol to obtain a stock solution of 1 mg/mL. 16, 32, 64, 96, and 120 mg of HNTs were dispersed in 4 mL of 1 mg/mL of naringenin solution. The suspension was sonicated for 30 minutes and then subjected to a vacuum (22 mmHg). Vacuum suction was performed for 30 minutes and then suspension was kept at atmospheric pressure for 10 minutes. 3 vacuum suction and release cycles were performed for drug loading. Under vacuum, the solvent was evaporated.

Encapsulation and loading capacity

Dry powder was ground and washed with absolute ethanol. The free drug was separated by centrifuging naringenin-loaded HNTs at 8000 rpm for 20 min. The supernatant was analyzed by UV/Vis at an absorbance wavelength of 290 nm to calculate the encapsulation efficiency and loading capacity.

$$\text{Encapsulation efficiency (EE) (\%)} = \frac{Wt}{W0} \times 100$$

Wt=the mass of the loaded drug
W0= the total mass of the drug used for loading

$$\text{Loading capacity (\%)} = \frac{Wt}{WH+Wt} \times 100$$

Wt= the mass of the loaded drug
WH= the total mass of HNTs

The concentrations of 5, 10, 12.5.15, 20 µg/mL of naringenin in absolute ethanol were prepared and used for UV/Vis analysis of naringenin by UV/Vis spectrophotometer (Optizen 2120 uv Plus, Mecasys, Korea) for drawing the standard curve. The standard curve was used to calculate encapsulation efficiency and loading capacity.

Encapsulation efficiency and loading capacity were also analyzed by the Waters Alliance HPLC system (USA) that consisted of a Waters 2695 separations module, a Waters 2487 dual absorbance detector (UV/Vis), and a Waters 717 plus autosampler. The column which was used for analysis was a C18 (symmetry, 4.6×250 mm, 5 µm). The mobile phase composition was methanol:water (3:1 v/v) with 0.5 % v/v acetic acid. The mobile phase flow rate and the column temperature were adjusted at 1 mL/min and 25 °C. The injection volume was 20 µl. Naringenin was detected at an absorbance wavelength of 290 nm and temperature of 25 °C [10].

Scanning electron microscope (SEM) analysis

The surface morphology of HNTs and naringenin-loaded HNTs (The HNTs:drug ratio of 4 w/w) were studied by SEM (Zeiss, DSM-960A, Germany). The samples were dispersed in water by sonication and a drop of each sample was placed on a slide and then covered by a gold thin layer after drying.

Fourier transform infrared spectroscopy (FTIR) analysis

The FTIR spectra of naringenin, HNTs, and drug-loaded HNTs (The HNT:drug ratio of 4 w/w) were recorded by Frontier PerkinElmer (USA). The scanning was done in the range 400–4000 cm−1 with the speed of 2 mm/s at room temperature.

Differential scanning calorimetry (DSC) analysis

An appropriate amount of each sample (naringenin, HNTs, and drug-loaded HNTs (The HNT:drug ratio of 4 w/w)) was sealed in aluminum pans and heated from 25 °C to 350 °C in the argon atmosphere (Q600, TA, USA) with a heating rate of 10 °C/min $^{-1}$.

X-ray diffraction (XRD) analysis

Naringenin, HNTs and naringenin-loaded HNTs (The HNTs:drug ratio of 4 w/w) were analyzed by the XRD technique. The XRD data were obtained using a Philips diffractometer (X'Pert MPD, Netherlands). The scanning was performed from 5° to 80° 2ɵ and at a speed of 1°/min.

Drug release experiment

In vitro release of naringenin from free drug solution and drug-loaded HNTs (The HNT:drug ratio of 4 w/w) was determined by a dialysis technique. Drug-loaded HNTs (10 mg) was placed in a dialysis bag (12-14 KD). The dialysis bags containing free drug solution and drug-loaded HNTs were immersed in 100 mL of phosphate buffer saline (PBS) with pH 7.4 at 37 °C. At defined time intervals, 2 mL of dissolution medium was collected and analyzed for naringenin content and 2 mL of fresh medium was replaced. The naringenin content of the dissolution medium was analyzed by UV/Vis and HPLC as described earlier.

Measurement of antioxidant activity of naringenin

The scavenging activity of free radicals by naringenin was evaluated by DPPH assay. Initially, 0.2 mM solution of DPPH in ethanol was prepared, then different concentrations of naringenin in ethanol were prepared. 2 mL of drug solution was mixed with 1 mL DPPH solution in each vial. The final drug concentrations were 100, 200, 300, 400, 500 and 750 µg/mL. 2 mL of ethanol was mixed with 1 mL DPPH and used as control. After 2 h, the absorbance was recorded at 517 nm.

To evaluate the effect of drug loading in HNTs on drug solubility and the antioxidant activity of naringenin, initially 100 µl of the drug solution in ethanol was mixed with 2.5 mL of purified water, then 400 µl DPPH in ethanol (0.5 mM) was added to it. The final concentration of the drug was 750 µg/mL in the vial. The amount of nanocomposite was weighted (containing 2.25 mg drug), and then dispersed in 2.5 mL water. Next, 100 µl ethanol was added and mixed, and then 400 µl DPPH in ethanol (0.5 mM) was added and mixed. After 2 hr, the absorbance was recorded.

DPPH radical scavenging activity (%) = (Ac-As)/Ac ×100

Where Ac stands for the absorbance of the control and As is the absorbance of the drug solution.

Cytotoxicity assay

The cells at density of 1×104 cells per well were seeded in 96 well plates and incubated for 24 h at 37 °C in a humidified 5% CO2 incubator. After incubation, the cells were treated with free naringenin, HNTs, and naringenin-loaded HNTs (The HNT:drug ratio of 4 w/w). The concentrations of naringenin for both free naringenin and

naringenin-loaded HNTs were 10, 20, and 30 µg/mL. The HNTs concentrations for HNTs and drug-loaded HNTs were equal. After 24 h, the media were removed and the cells were washed with cold PBS (2 times). Then, 100 µL of MTT solution was added to each well, and the cells were incubated for the next 4 hr in the incubator. The formazan crystals were dissolved in DMSO and the absorbance was read at 570 nm using a microplate reader (Awareness). Using the following formula the percentage of cell viability was calculated:

$$\text{Cell viability (\%)} = (At/Ac) \times 100$$

Which At was the absorbance of each treatment and the Ac was the absorbance of cells with no treatment. The test was performed in triplicate.

Statistical analysis

Statistical analysis was performed using GraphPad Prism version 8 (GraphPad Software, San Diego, CA) and OriginPro version 8.6 (Northampton, MA 01060 USA). Analysis of variance (ANOVA) test was performed for determination of statistical significance of Figure 8b. Statistical significance of Figure 9 was determined by ANOVA test, followed by Tukey test.

RESULT AND DISCUSSION

Encapsulation efficiency and loading capacity

Encapsulation efficiency and loading capacity were analyzed by HPLC and UV/Vis. Fig. 1 shows the HPLC chromatogram overlay of naringenin before and after drug loading that indicated the drug remains pure and stable during the whole process.

By increasing the HNTs: drug ratio (w/w), the encapsulation efficiency was increased, but loading capacity was decreased. The highest encapsulation efficiency was 87.7 ±5% for the HNTs:drug ratio of 30 (w/w). The encapsulation efficiency of the formulations with the HNTs:drug ratios of 24, 16, 8 and 4 was 82.1 ±3.4%, 72.9 ± 4%, 63 ±3.2% and 54.8 ±3%, respectively. By decreasing the HNTs:drug ratio, the loading capacity was increased. The highest loading capacity (12 ± 0.6%) corresponded to the formulation with the HNTs:drug ratio of 4 w/w. The loading capacity of the formulations with the HNTs:drug ratios of 8, 16, 24, and 30 was 7.3 ± 0.3%, 4.3 ± 0.2%, 3.3 ± 0.1%, and 2.8 ± 0.2%, respectively (Fig. 2). In a previous study, curcumin was loaded in HNT-NH2, HNTs, and HNT-g-CS (chitosan grafted halloysite) at various HNTs:drug ratios (50, 25, and 10 w/w). At a 50:1 ratio, maximum encapsulation efficiency (90.8%) and the lowest loading capacity (about 0.9%) for HNT-g-CS was obtained. By decreasing the HNTs:drug ratio, the entrapment efficiency was decreased and loading capacity was increased. At the HNTs:drug ratio of 10, maximum loading capacity (3.4%), and the lowest encapsulation efficiency (65%) were obtained. Similar results for HNTs-NH2 and HNTs were observed [30].

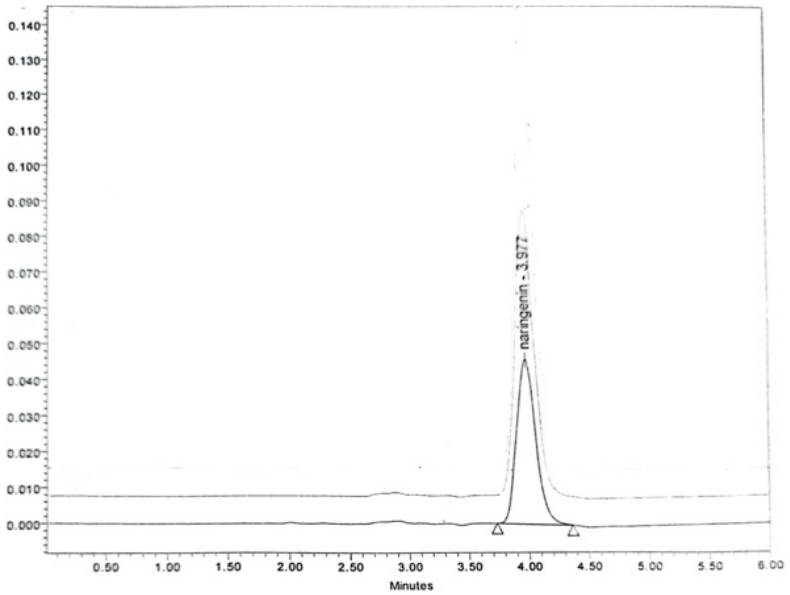

Fig. 1 The HPLC chromatogram overlay of naringenin after and before drug loading (The HNTs: drug ratio of 4 w/w).S

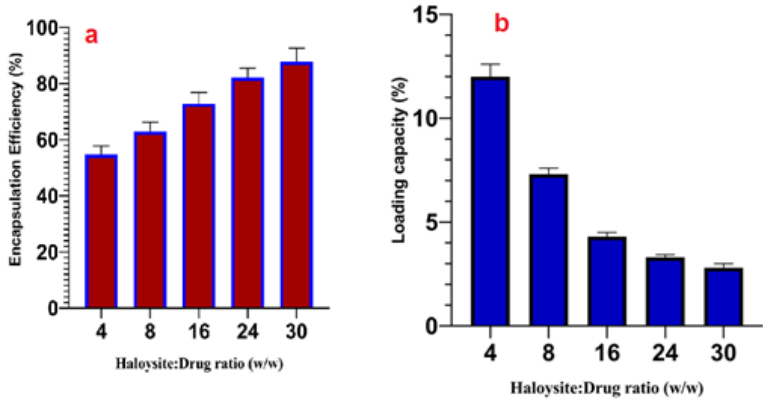

Fig. 2. The relation between encapsulation efficiency and HNTs:drug ratio (w/w) (a), loading capacity and HNTs:drug ratio (w/w) (b). Each data represents mean ±SD (n=3).

Morphology study

The SEM analysis was used for the morphological study (Fig. 3). SEM images showed the tubular and cylindrical shapes of HNTs. This morphology was also observed after drug loading process and the morphology was unchanged. This situation was also reported in another study [29]. Particle size distribution histograms of HNTs (Fig. 3c) and naringenin-loaded HNTs (Fig. 3d) indicate that the mean diameters of HNTs and naringenin-loaded HNTs are 70.19 nm and 76.34 nm, respectively.

DSC analysis

In the first step, the DSC curve of naringenin indicated weight loss, which was attributed to residual solvent (drug loading process) or adsorbed moisture in naringenin-loaded HNTs at the temperature range of 50-150 °C [31]. The melting point of naringenin was observed at 256.14 °C in its DSC curve. The endothermal peak attributed to the melting point of naringenin disappeared in

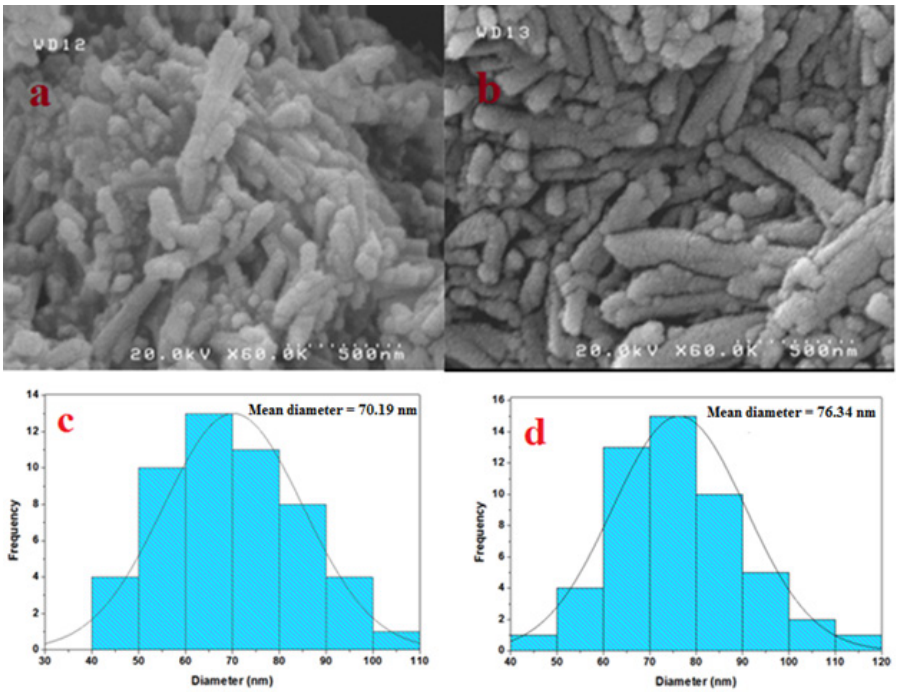

Fig. 3. SEM images of HNTs (a) and naringenin- loaded HNTs (b). Particle size distribution histograms of HNTs (c) and naringenin-loaded HNTs (d) were determined from the SEM images

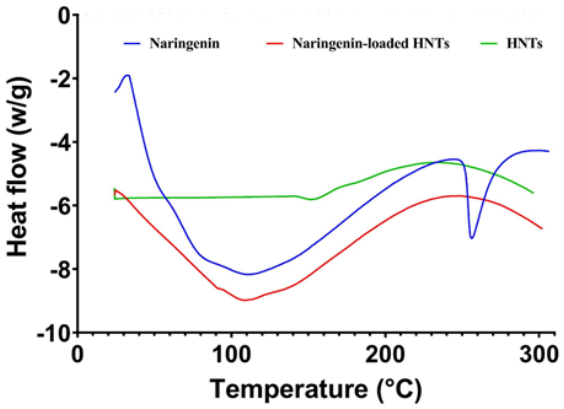

Fig. 4. DSC analysis of naringenin, HNTs and naringenin- loaded HNTs (The HNT:drug ratio of 4 w/w).

the DSC curve of naringenin-loaded HNTs (Fig. 4). Disappearance of the melting point of naringenin in naringenin-loaded HNTs may be attributed to molecular dispersion of naringenin in HNTs and the transformation of naringenin crystalline form to its amorphous form [10, 15, 17]. In a previous study, DSC analysis of naringenin-loaded chitosan-dextran sulfate nanocarrier was studied. Crystalline naringenin exhibited a sharp peak at 250 °C. This sharp peak which was called the melting point of naringenin was disappeared in the naringenin-loaded carrier. The reason for the disappearance of this peak was also related to the homogeneous dispersion of naringenin in the polymer matrix [31]. The study of DSC analysis of naringenin-loaded sulfobutylether-β-cyclodextrin/ chitosan nanoparticles indicated that melting point of naringenin (sharp peak at 258 °C in naringenin DSC) was disappeared. Amorphous dispersion of naringenin in carrier resulted in disappearance of naringenin melting point [17]. DSC analysis of naringenin, naringenin-loaded SLN, and their physical mixture showed that the melting point of naringenin (258.17 °C) was disappeared in naringenin-loaded SLN. The absence of this peak was attributed to the amorphous and molecular state of the drug after its loading. However, their physical mixture showed the melting point of naringenin at 232.17 °C [10]. DSC analysis of the complex of naringenin with Hydroxypropyl-β-Cyclodextrin (HP-β-CD), naringenin, and their physical mixture was studied. The melting point of naringenin appeared at a temperature of 251.1 °C. The effect of both naringenin and HP-β-CD was observed in their physical mixture. However, the naringenin melting point was disappeared in their complex. The disappearance of the peak was attributed to the complete dispersion of the drug and its interaction with HP-β-CD [15].

XRD analysis

XRD of naringenin, HNTs and naringenin-loaded HNTs was studied. XRD analysis was used to investigate the crystalline structure before and after drug loading. Diffraction peaks at 2ɵ of 11.9°, 20°, 24.6°, 35.01°, 38.01°, 54.7°, and 62.46° were observed in the HNTs XRD analysis, which is in agreement with other studies [32-34]. The presence of sharp diffraction peaks between 3° and 40° 2ɵ in naringenin XRD analysis (Fig. 5) are attributed to a well crystallized form of naringenin [10, 35]. The XRD analysis of naringenin-loaded HNTs was similar to HNTs and diffraction peaks in the XRD analysis of naringenin disappeared in the XRD analysis of naringenin-loaded HNTs (Fig. 5). The diffraction peaks disappearance was attributed to naringenin dispersion at the molecular level in the HNTs structure [36]. In another study, chlorhexidine was loaded in HNTs. The sharp and narrow diffraction peaks of chlorhexidine indicated the highly crystalline structure of chlorhexidine. These diffraction peaks were disappeared in chlorhexidine-loaded HNTs that confirmed uniform chlorhexidine loading in the HNTs structure, demonstrating successful loading of chlorhexidine [37]. Four model drugs (verapamil HCl, flurbiprofen, atenolol, and furosemide) were loaded in HNTs. Characteristic peaks in XRD analysis of these drugs were disappeared in drug-loaded HNTs because drug loading resulted in property transformation from crystalline to amorphous state [38]. In a study, breviscapine was loaded in HNTs. The breviscapine's diffraction peaks were absent in breviscapine-loaded HNTs and XRD analysis of HNTs and breviscapine-loaded HNT were similar.

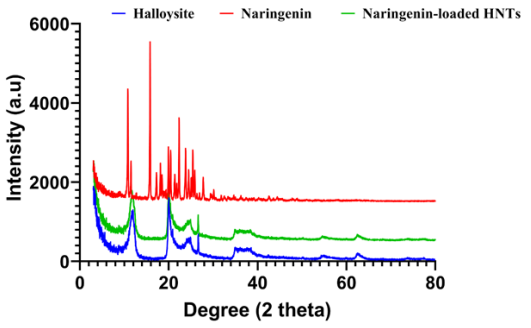

Fig. 5. XRD analysis of naringenin, HNTs and naringenin-loaded HNTs (The HNT:drug ratio of 4 w/w).

Successful loading of breviscapine in HNTs resulted in the disappearance of breviscapine's diffraction peaks [39]. The comparison of XRD analysis of naringenin, HPβCD, and naringenin loaded-HPβCD showed that naringenin loading in HPβCD resulted in no detection diffraction peaks of naringenin in naringenin- encapsulated HPβCD [15]. In another study, XRD analysis of naringenin, SLN, and naringenin-loaded SLN was studied. Characteristic peaks of naringenin were absent in naringenin-loaded SLN because of its transformation from crystalline state to amorphous [10]. In another study, the crystalline peaks which were observed in curcumin, had disappeared in curcumin loaded HNTs. Loading curcumin in HNTs was the reason for this disappearance [40].

FTIR analysis

The FTIR analysis of naringenin, HNTs, and naringenin-loaded HNTs are presented in Fig. 6. The characteristic peaks at 3695 and 3626 cm^{-1} in FTIR analysis of HNTs and naringenin–loaded HNTs are corresponding to the stretching vibration of the inner surface hydroxyl groups of the HNTs. The peaks at 910 and 1035 cm^{-1} in FTIR analysis of HNTs and naringenin–loaded HNTs represents Al-OH bending and Si-O-Si symmetric stretching [29]. FTIR analysis of naringenin showed several characteristic bands; 1600-1900 cm^{-1} are bands corresponding to –C=O stretching, and the band corresponding to C-O stretching are bands in the range of 1080-1250 cm^{-1}. The characteristic band in the range of 3100-3290 cm^{-1} corresponds to O-H stretching, and the characteristic peak of C-C is 1150 cm^{-1}. The characteristic bands in the range of 1450-1630 cm^{-1} is corresponding to C=C stretching. The bands in range of 2830 – 3100 cm^{-1} are corresponding to -CH, -CH2, -CH3 stretching [7]. The characteristic peaks of naringenin (1464, 1631, 1520, 1602 cm^{-1}) were also identified in naringenin-loaded HNTs. Identification of naringenin peaks in naringenin-loaded HNTs indicated that naringenin was successfully loaded into HNTs, proving the chemical stability of naringenin in HNTs [10].

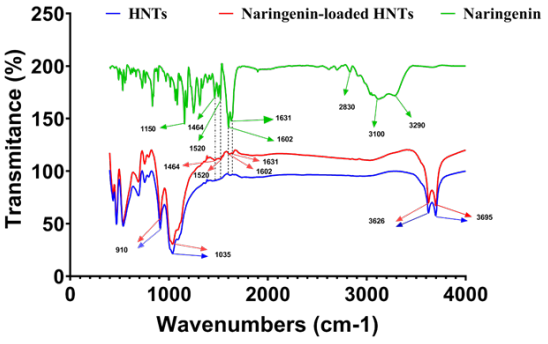

Fig. 6. FTIR analysis of naringenin, naringenin- loaded HNTs (The HNT:drug ratio of 4 w/w) and HNTs

Drug release study

Drug release percentage from naringenin-loaded HNTs after 24 hr was 67 ±5%. Fick's first law of diffusion say that the diffusion rate is proportional to the concentration gradient. Burst release which was observed in the initial stages may be attributed to high concentration of naringenin [29]. Burst release of naringenin was followed by sustained release. Drug release experiment from free drug solution indicated rapid drug release. After 5 hr, the amount of drug release percentage from free drug solution was 100% (Fig. 7). A comparison of drug release percentage from loaded drug and free drug solution indicates that drug loading resulted in controlled drug release. Fitting models for the results that were obtained from the drug release study (naringenin–loaded HNTs) were investigated by zero-order, first-order, Higuchi, Hixon-Crowell square-root, and Korsmeyer-Peppas kinetic models. The highest correlation coefficient was obtained from fitting data in the Korsmeyer-Peppas model (R^2= 0.97). The value of the release exponent (n) is less than 0.45 indicating a diffusion-controlled drug release mechanism and the drug release follows fickian release behavior from HNTs [29, 41-43].

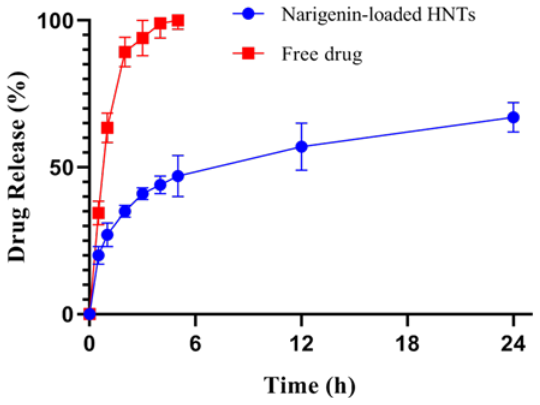

Fig. 7. Drug release from free drug solution and naringenin -loaded HNTs (The HNT:drug ratio of 4 w/w). Each data represents mean ±SD (n=3).

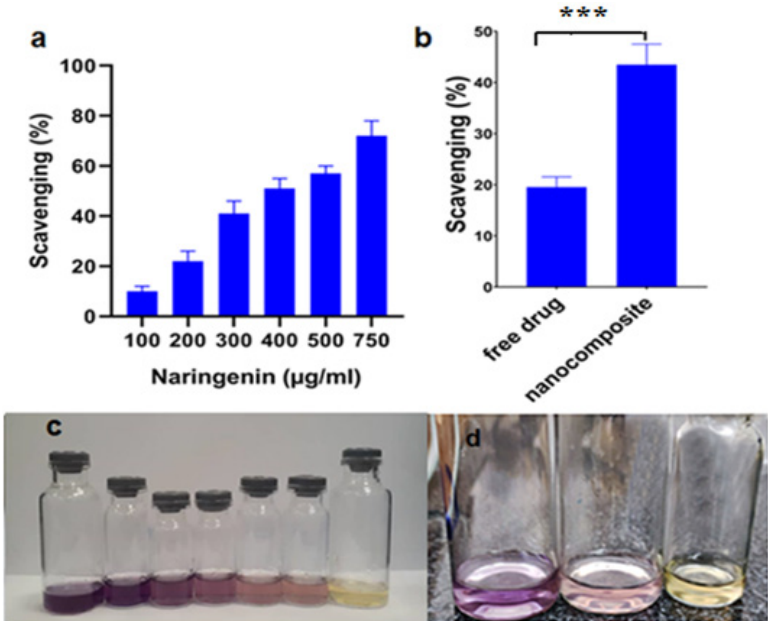

Fig. 8. Investigation of antioxidant activity of naringenin by DPPH assay in the different concentrations (a), investigation of antioxidant activity of naringenin- loaded HNTs (The HNT:drug ratio of 4 w/w) and free naringenin in the naringenin concentration of 750 µg/ml (b), the color change of DPPH solution in the different concentrations of naringenin (left to right (blank, 100, 200, 300,400, 500, 750 µg/mL)) (c), the comparison of the color change of DPPH solution after reaction with naringenin-loaded HNTs and free naringenin (left to right (blank, free drug, nanocomposite) in the aqueous phase (d). Each data represents mean ±SD (n=3). *** *P*< 001.

Measurement of antioxidant activity of naringenin

In 100, 200, 300, 400, 500 and 750 µg/mL concentrations, naringenin activity for DPPH scavenging was investigated. By increasing naringenin concentration, DPPH scavenging was increased. Naringenin showed antioxidant activity by scavenging DPPH radicals with an IC50 value of 400 ±4 µg/mL (Fig. 8a). The color of the DPPH solution after reaction with naringenin was changed to yellow, and by increasing the naringenin concentration, the color change to yellow was enhanced (Fig. 8c). Poor solubility of naringenin, restricts its bioavailability and antioxidant activity. Naringenin was loaded in HNTs to increase naringenin solubility, and thereby, its antioxidant activity. For the first time, in the present study, the effect of drug loading in nanoparticles on drug solubility by an innovative change in DPPH assay was investigated. Interestingly, the antioxidant activity of drug-loaded HNTs (43.49 ± 4%) was significantly more than free drug solution (19.53 ± 2 %) (Fig. 8b). Due to the poor solubility of naringenin most of the free drug was not soluble in the aqueous phase, and subsequently showed low antioxidant activity, but HNTs increased the solubility of naringenin in the aqueous phase, and, in turn, the antioxidant activity of the drug. Thus, drug loading in HNTs improves naringenin solubility and antioxidant activity. Fig. 8d shows that naringenin-loaded HNTs had higher ability to change the color of the DPPH solution to yellow, in comparison with the free drug.

Cell toxicity

Cytotoxicity of HNTs, naringenin, and naringenin-loaded HNTs in the cancer cell lines of HT-29 (fig 9a) and MCF-7 (fig 9b) was investigated by MTT assay. Cell viability of both cell lines for naringenin-loaded HNTs was significantly lower than free naringenin (Fig. 9). Loading of naringenin in HNTs enhanced its anticancer property. Higher cell toxicity of naringenin-loaded HNTs in comparison with free naringenin may be attributed to enhanced solubility of naringenin after loading in HNTs [25], higher uptake ability of HNTs [44], the gradual release followed by longer exposure of the cells to the drug for a longer prolonged period [44, 45], and also, the possible cytotoxicity of HNTs [46].

CONCLUSION

Due to the low solubility and low bioavailability of naringenin, HNTs were used for the delivery

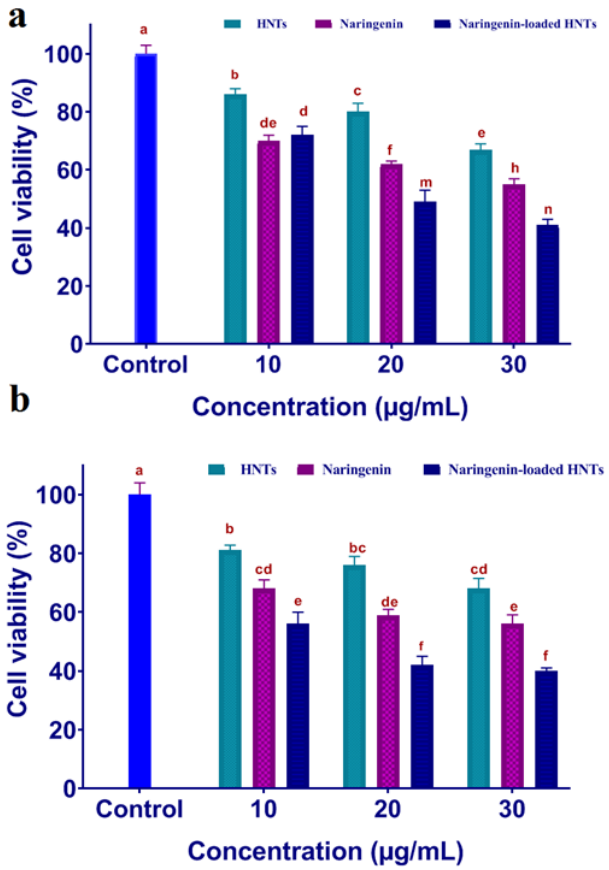

Fig. 9. Cytotoxicity of naringenin, naringenin-loaded HNTs (The HNT:drug ratio of 4 w/w) and HNTs on the HT-29 (a) and MCF-7 cells (b). Each data represents mean ±SD (n=3). Statistical significance was determined by ANOVA followed by Tukey test. Different letters indicate significant differences among different groups (P< 0.05).

of naringenin. Naringenin was loaded in HNTs at different HNTs:drug ratios (4, 8, 16, 24, and 30 w/w). By increasing the HNTs:drug ratio, the encapsulation efficiency increased, but the loading capacity was decreased. FTIR, DSC, and XRD confirmed the drug loading. A drug release study indicated controlled drug release from naringenin-loaded HNTs. DPPH assay indicated the high antioxidant activity of naringenin. Loading of naringenin in HNTs resulted in enhanced solubility of naringenin and, subsequently, more inhibition of DPPH in comparison with free naringenin. Naringenin-loaded HNTs decreased the cell viability of the HT-29 and MCF-7 cell lines compared to free naringenin. In conclusion, HNTs can be a good candidate for the delivery of naringenin.

ACKNOWLEDGMENTS

The authors would like to acknowledge the financial support of University of Tehran, Tehran, Iran.

FUNDING

No funding was received.

ETHICS APPROVAL AND CONSENT TO PARTICIPATE

Not applicable.

AVAILABILITY DATA AND MATERIALS

Data will be provided upon request.

CONFLICTS OF INTERESTS

The authors declare that they have no competing interests.

REFERENCES

1. Kawaii S, Tomono Y, Katase E, Ogawa K, Yano M. Quantitation of flavonoid constituents in citrus fruits. J Agric Food Chem. 1999;47(9):3565-3571.
2. Nogata Y, Sakamoto K, Shiratsuchi H, Ishii T, Yano M, Ohta H. Flavonoid composition of fruit tissues of citrus species. Biosci Biotechnol Biochem. 2006;70(1):178-192.
3. Lee C-H, Jeong T-S, Choi Y-K, Hyun B-H, Oh G-T, Kim E-H, et al. Anti-atherogenic effect of citrus flavonoids, naringin and naringenin, associated with hepatic ACAT and aortic

VCAM-1 and MCP-1 in high cholesterol-fed rabbits. Biochem Biophys Res Commun. 2001;284(3):681-688.
4. Verhoeyen M, Bovy A, Collins G, Muir S, Robinson S, De Vos C, et al. Increasing antioxidant levels in tomatoes through modification of the flavonoid biosynthetic pathway. J Exp Bot. 2002;53(377):2099-2106.
5. Arul D, Subramanian P. Inhibitory effect of naringenin (citrus flavonone) on N-nitrosodiethylamine induced hepatocarcinogenesis in rats. Biochem Biophys Res Commun. 2013;434(2):203-209.
6. Jayachitra J, Nalini N. Effect of naringenin (citrus flavanone) on lipid profile in ethanol-induced toxicity in rats. J Food Biochem. 2012;36(4):502-511.
7. Kumar SP, Birundha K, Kaveri K, Devi KR. Antioxidant studies of chitosan nanoparticles containing naringenin and their cytotoxicity effects in lung cancer cells. Int J Biol Macromol. 2015;78:87-95.
8. Hsiu S-L, Huang T-Y, Hou Y-C, Chin D-H, Chao P-DL. Comparison of metabolic pharmacokinetics of naringin and naringenin in rabbits. Life Sci. 2002;70(13):1481-1489.
9. Yen F-L, Wu T-H, Lin L-T, Cham T-M, Lin C-C. Naringenin-loaded nanoparticles improve the physicochemical properties and the hepatoprotective effects of naringenin in orally-administered rats with CCl4-induced acute liver failure. Pharm Res. 2009;26(4):893-902.
10. Ji P, Yu T, Liu Y, Jiang J, Xu J, Zhao Y, et al. Naringenin-loaded solid lipid nanoparticles: preparation, controlled delivery, cellular uptake, and pulmonary pharmacokinetics. Drug Des Devel Ther. 2016;10:911.
11. Teixeira M, Pedro M, Nascimento MSJ, Pinto MM, Barbosa CM. Development and characterization of PLGA nanoparticles containing 1, 3-dihydroxy-2-methylxanthone with improved antitumor activity on a human breast cancer cell line. Pharm Dev Technol. 2019;24(9):1104-1114.
12. Simeonova S, Georgiev P, Exner KS, Mihaylov L, Nihtianova D, Koynov K, et al. Kinetic study of gold nanoparticles synthesized in the presence of chitosan and citric acid. Colloids Surf A Physicochem Eng Asp. 2018;557:106-115.
13. Crivelli B, Bari E, Perteghella S, Catenacci L, Sorrenti M, Mocchi M, et al. Silk fibroin nanoparticles for celecoxib and curcumin delivery: ROS-scavenging and anti-inflammatory activities in an in vitro model of osteoarthritis. Eur J Pharm Biopharm. 2019;137:37-45.
14. Krishnakumar N, Sulfikkarali N, RajendraPrasad N, Karthikeyan S. Enhanced anticancer activity of naringenin-loaded nanoparticles in human cervical (HeLa) cancer cells. Biomedicine & preventive nutrition. 2011;1(4):223-231.
15. Wen J, Liu B, Yuan E, Ma Y, Zhu Y. Preparation and physicochemical properties of the complex of naringenin with hydroxypropyl-β-cyclodextrin. Molecules. 2010;15(6):4401-4407.
16. Semalty A, Semalty M, Singh D, Rawat M. Preparation and characterization of phospholipid complexes of naringenin for effective drug delivery. J Incl Phenom Macrocycl Chem. 2010;67(3):253-260.
17. Zhang P, Liu X, Hu W, Bai Y, Zhang L. Preparation and evaluation of naringenin-loaded sulfobutylether-β-cyclodextrin/chitosan nanoparticles for ocular drug delivery. Carbohydr Polym. 2016;149:224-230.
18. R. Price BG, Y. Lvov, R. In-vitro release characteristics of tetracycline HCl, khellin and nicotinamide adenine dineculeotide from halloysite; a cylindrical mineral. J Microencapsul 2001;18(6):713-722.
19. Veerabadran NG, Price RR, Lvov YM. Clay nanotubes for encapsulation and sustained release of drugs. Nano. 2007;2(02):115-120.
20. Wei W, Minullina R, Abdullayev E, Fakhrullin R, Mills D, Lvov Y. Enhanced efficiency of antiseptics with sustained release from clay nanotubes. RSC Adv. 2014;4(1):488-494.
21. Tan D, Yuan P, Annabi-Bergaya F, Yu H, Liu D, Liu H, et al. Natural halloysite nanotubes as mesoporous carriers for the loading of ibuprofen. Microporous Mesoporous Mater. 2013;179:89-98.
22. Lun H, Ouyang J, Yang H. Natural halloysite nanotubes modified as an aspirin carrier. **RSC** Adv. 2014;4(83):44197-44202.
23. Dionisi C, Hanafy N, Nobile C, De Giorgi ML, Rinaldi R, Casciaro S, et al. Halloysite clay nanotubes as carriers for curcumin: characterization and application. IEEE Trans Nanotechnol 2016;15(5):720-724.
24. Hemmatpour H, Haddadi-Asl V, Roghani-Mamaqani H. Synthesis of pH-sensitive poly (N, N-dimethylaminoethyl methacrylate)-grafted halloysite nanotubes for adsorption and controlled release of DPH and DS drugs. Polymer. 2015;65:143-153.
25. Riela S, Massaro M, Colletti CG, Bommarito A, Giordano C, Milioto S, et al. Development and characterization of co-loaded curcumin/triazole-halloysite systems and evaluation of their potential anticancer activity. Int J Pharm. 2014;475(1-2):613-623.
26. Wang Q, Zhang J, Zheng Y, Wang A. Adsorption and release of ofloxacin from acid-and heat-treated halloysite. Colloids Surf B Biointerfaces. 2014;113:51-58.
27. Wang Q, Zhang J, Wang A. Alkali activation of halloysite for adsorption and release of ofloxacin. Appl Surf Sci. 2013;287:54-61.
28. Aguzzi C, Viseras C, Cerezo P, Salcedo I, Sánchez-Espejo R, Valenzuela C. Release kinetics of 5-aminosalicylic acid from halloysite. Colloids Surf B Biointerfaces. 2013;105:75-80.
29. Nyankson E, Aboagye SO, Efavi JK, Agyei-Tuffour B, Paemka L, Asimeng BO, et al. Chitosan-Coated Halloysite Nanotubes As Vehicle for Controlled Drug Delivery to MCF-7 Cancer Cells In Vitro. Materials (Basel). 2021;14(11):2837.
30. Liu M, Chang Y, Yang J, You Y, He R, Chen T, et al. Functionalized halloysite nanotube by chitosan grafting for drug delivery of curcumin to achieve enhanced anticancer efficacy. J Mater Chem B. 2016;4(13):2253-2263.
31. Muralidharan S, Shanmugam K. Synthesis and Characterization of Naringenin-Loaded Chitosan-Dextran Sulfate Nanocarrier. J Pharm Innov. 2021;16(2):269-278.
32. Cheng C, Gao Y, Song W, Zhao Q, Zhang H, Zhang H. Halloysite nanotube-based H2O2-responsive drug delivery system with a turn on effect on fluorescence for real-time monitoring. Chem Eng J. 2020;380:122474.
33. Pandey G, Munguambe DM, Tharmavaram M, Rawtani D, Agrawal Y. Halloysite nanotubes-An efficient 'nano-support'for the immobilization of α-amylase. Appl Clay Sci. 2017;136:184-191.
34. Liu Y, Zhang J, Guan H, Zhao Y, Yang J-H, Zhang B. Preparation of bimetallic Cu-Co nanocatalysts on poly (diallyldimethylammonium chloride) functionalized halloysite nanotubes for hydrolytic dehydrogenation of ammonia borane. Appl Surf Sci. 2018;427:106-113.
35. Guan M, Shi R, Zheng Y, Zeng X, Fan W, Wang Y, et al. Characterization, *in vitro* and *in vivo* evaluation of naringenin-hydroxypropyl-β-cyclodextrin inclusion for pulmonary delivery. Molecules. 2020;25(3):554.
36. Rao KM, Nagappan S, Seo DJ, Ha C-S. pH sensitive halloysite-sodium hyaluronate/poly (hydroxyethyl methacrylate) nanocomposites for colon cancer drug delivery. Appl Clay Sci. 2014;97:33-42.
37. Barot T, Rawtani D, Kulkarni P. Development of chlorhexidine

loaded halloysite nanotube based experimental resin composite with enhanced physico-mechanical and biological properties for dental applications. J Compos Sci. 2020;4(2):81.
38. Husain T, Shoaib MH, Ahmed FR, Yousuf RI, Farooqi S, Siddiqui F, et al. Investigating halloysite nanotubes as a potential platform for oral modified delivery of different BCS class drugs: characterization, optimization, and evaluation of drug release kinetics. Int J Nanomedicine. 2021;16:1725.
39. Gao M, Lu L, Wang X, Lin H, Zhou Q, editors. Preparation of a novel breviscapine-loaded halloysite nanotubes complex for controlled release of breviscapine. IOP Conf Ser Mater Sci Eng. 2017: IOP Publishing.
40. Siva Gangi Reddy N, Madhusudana Rao K, Park SY, Kim T, Chung I. Fabrication of aminosilanized halloysite based floating biopolymer composites for sustained gastro retentive release of curcumin. Macromol Res. 2019;27(5):490-496.
41. Permanadewi I, Kumoro A, Wardhani D, Aryanti N, editors. Modelling of controlled drug release in gastrointestinal tract simulation. J Phys Conf Ser. 2019: IOP Publishing.
42. Ghalandari B, Divsalar A, Komeili A, Eslami-Moghadam M, Saboury AA, Parivar K. Mathematical analysis of drug release for gastrointestinal targeted delivery using β-lactoglobulin nanoparticle. Biomacromol J. 2015;1(2):204-211.
43. Bediako EG, Nyankson E, Dodoo-Arhin D, Agyei-Tuffour B, Łukowiec D, Tomiczek B, et al. Modified halloysite nanoclay as a vehicle for sustained drug delivery. Heliyon. 2018;4(7).
44. Yamina AM, Fizir M, Itatahine A, He H, Dramou P. Preparation of multifunctional PEG-graft-halloysite nanotubes for controlled drug release, tumor cell targeting, and bio-imaging. Colloids Surf B Biointerfaces. 2018;170:322-329.
45. Hamedi S, Koosha M. Designing a pH-responsive drug delivery system for the release of black-carrot anthocyanins loaded in halloysite nanotubes for cancer treatment. Appl Clay Sci. 2020;197:105770.
46. Li W, Liu D, Zhang H, Correia A, Mäkilä E, Salonen J, et al. Microfluidic assembly of a nano-in-micro dual drug delivery platform composed of halloysite nanotubes and a pH-responsive polymer for colon cancer therapy. Acta Biomater. 2017;48:238-246.